Wearable Pressure Sensors Based on Carbonized Graphene Coated Waste Paper Aerogel

Ang Li
Sichuan University
Ce Cui
Sichuan University
Weijie Wang
Sichuan University
Yue Zhang
Sichuan University
Jianyu Zhai
Sichuan University
Ronghui Guo (ronghuiguo214@126.com)
Sichuan University
Shaojian Lin
Sichuan University
Wenfeng Qin
Civil Aviation Flight University of China
Erhui Ren
Sichuan University
Hongyan Xiao
Sichuan University
Mi Zhou
Sichuan University
Jinwei Zhang
Sichuan University

Research Article

Keywords: Wearable pressure sensor, aerogel, graphene, waste paper, atmospheric drying

Posted Date: August 4th, 2021

DOI: https://doi.org/10.21203/rs.3.rs-741840/v1

Abstract

Graphene is complexed with cellulose fibers to construct 3D aerogels, which is generally considered to be an environmentally friendly and simple strategy to achieve wide sensing, high sensitivity and low detection of wearable piezoresistive pressure sensors. Here, graphene is incorporated into waste paper fibers with cellulose as the main component to prepare graphene coated waste paper aerogel (GWA) using a simple “filtration-oven drying” method under atmospheric pressure. The GWA was further annealed to obtain the carbonized graphene coated waste paper aerogel (C-GWA) to achieve low density and excellent resilience. The result shows that the C-GWA has a rough outer surface due to the 3D structure formed by interpenetrated fibers and the carbon skeleton with wrinkles. The sensor based on GCA shows low density (25mg/cm^3), a wide detection range of 0-132 kPa, an ultra-low detection limit of 2.5 Pa (a green bean, ≈ 53.4 mg), and a high sensitivity of 31.6 kPa^{-1}. In addition, the sensor based on C-GWA with the excellent performance can be used to detect human motions including the pulse of the human body, cheek blowing and bending of human joints. The result indicates that the sensor based on C-GWA shows great potential for wearable electronic products.

1 Introduction

In recent years, wearable pressure sensors have been potentially applied in the fields of electronic skin(Cao et al. 2021), software robots(Zhan et al. 2017) and human health monitoring(Chen et al. 2020a; Zhang et al. 2020a). Piezoresistive pressure sensors have attracted great attention due to their easy preparation, simple readout mechanism, low power consumption and convenient signal acquisition(Huang et al. 2021a; Peng et al. 2020). In practical application, wearable pressure sensors with ultra-low detection limit, high sensitivity, wide detection range and long-term durability are very important(Wang et al. 2020). In order to realize the excellent performance of piezoresistive pressure sensors, the innovative structure strategy of constructing three-dimensional (3D) and porous conductive aerogels has been developed(Bi et al. 2020; Wang et al. 2020). These 3D and porous conductive aerogels have the advantages of large specific surface area, light weight, and large compressed space, and have become a promising material for wearable piezoresistive pressure sensors(Si et al. 2016; Xiao et al. 2019).

Excellent mechanical elasticity, high compressibility, and good conductivity are essential requirements for 3D and porous conductive aerogels that may be used in wearable pressure sensors(Ding et al. 2019). Functional soft materials (such as dimethyl siloxane (PDMS)(Sun et al. 2021b), polyurethane (PU)(Hodlur and Rabinal 2014) and polystyrene (PS)(Zhang et al. 2016)) as the skeleton to construct 3D and porous conductive aerogels is commonly used strategy to achieve the excellent mechanical elasticity and high compressibility of aerogels(Salzano de Luna et al. 2019). However, these petroleum-based functional soft materials are not only expensive, but also bring a series of environmental problems(Wei et al. 2021). In recent years, cellulose fibers as the skeleton to construct 3D and porous conductive aerogels have been widely used in wearable pressure sensors(Chen et al. 2020b; Wu et al. 2013). Cellulose fibers extracted from biomass materials contain absolute hydroxyl groups and a high aspect ratio, which contribute to the

formation of a stable 3D network structure(Chen et al. 2020c). Waste paper is a common biomass waste and the main component is cellulose. Nowadays, waste paper was mainly reused for paper pulp in paper-making industry. However, fiber strength of regenerated paper decreased gradually after recycling treatment and use(Li et al. 2018). Thus, new techniques for the applications of waste paper to produce high value-added products such as bioethanol(Al-Azkawi et al. 2019), gaseous fuels(Yamaguchi et al. 2010), oil absorbents(Jin et al. 2015), electrodes(Ye et al. 2015) has been developed. If waste paper fibers extracted from waste paper are used as the skeleton for constructing 3D porous conductive aerogels, not only the economic and environmental benefits improve, but also the aerogels show a stable 3D structure for pressure sensors.

The conductivity of 3D porous cellulose aerogels is usually achieved by incorporating conductive fillers into the aerogels(Huang et al. 2019). Carbon materials have excellent prospects due to their perfect conductivity and high chemical stability(Das et al. 2020). Graphene as one of carbon materials has the characteristics of high surface area, excellent mobility, high conductivity, good thermal conductivity and strong mechanical strength(Wei and Qu 2012), which are better than other carbon-based materials(Pang et al. 2018). Graphene can be incorporated into waste paper fibers to build a 3D porous conductive aerogel with good conductivity and stability. However, there are no reports about graphene incorporated into waste paper fibers to prepare aerogels for piezoresistive sensors.

In this work, waste paper fibers were extracted from waste paper, and graphene was wrapped on the surface to form graphene coated waste paper aerogel (GWA) using a simple “filtration-oven drying” method. In order to achieve low density and excellent resilience, the GWA was then annealed to obtain the carbonized graphene coated waste paper aerogel (C-GWA). The C-GWA shows low density, excellent compression resilience, wide sensing range, high sensitivity and low detection limit.

2 Experimental

2.1 Materials

Graphene was purchased from Yingxin Laboratory (Shanghai, China). Cetyl trimethyl ammonium bromide (CTAB), glacial acetic acid (CH_3COOH) and anhydrous ethanol were provided by Chengdu Kelong Chemical Reagent Co., Ltd. Sodium chlorite ($NaClO_2$) was provided by Shanghai Aladdin Biochemical Technology Co., Ltd. All the materials and agents were used as received without further purification treatment.

2.2 Preparation of waste paper fibers

10g of shredded printing waste paper was added into 1L of deionized water followed by vigorous magnetic stirring to form paper pulp. Subsequently, 0.14 mol $NaClO_2$ was dissolved in the pulp, and CH_3COOH was used to adjust the pH of the pulp to 4.5. The acidic pulp mixture had been stirred at 80°C for 2 h, and then washed with deionized water until pH 7. Finally, the neutral pulp was washed with

anhydrous ethanol to remove the water followed by drying in an oven under atmospheric pressure at 60°C to obtain waste paper fibers.

2.3 Preparation of carbonized graphene coated waste paper aerogels

0.06 g of CTAB powder was dissolved in 30 ml of anhydrous ethanol, and then 0.04 g of graphene was added, followed by sonicating for 2h to obtain the uniform ethanol dispersion of graphene. After that, 0.3 g of waste paper fibers were added to the ethanol dispersion of graphene, and then continuously stirred at high speed for 2 h to form homogeneous suspension. Afterward, the suspension was poured into a cylindraceous mould 20 mm in diameter, filtered to yield the wet aerogels with a height of 17 mm, and then dried in an oven under atmospheric pressure at 60°C to obtain the graphene coated waste paper aerogel (GWA). Finally, the GWA was annealed in a nitrogen atmosphere at 500°C with a heating rate of 3℃/min for 4 h to obtain the carbonized graphene coated waste paper aerogel (C-GWA). For comparison, the waste paper aerogel (WA) was also obtained by the filtration and oven drying under atmospheric pressure from waste paper fibers without graphene coating, and then directly annealed under same condition to obtain carbonized waste paper aerogels (C-WA).

2.4 Preparation of the wearable pressure sensors

The interdigital silver electrodes on the elastic tape were prepared by screen printing. Concretely, the conductive silver paste was squeezed onto the elastic tape through a screen printing plate with an interdigital pattern, followed by drying in an oven at 80°C for 2 h. Finally, C-GWA was adhered to the elastic tape with interdigitated electrodes on the surface.

2.5 Characterization

Field emission scanning electron microscope SEM (JEOL, JSM-5900LV) was used to characterize the morphology of C-WA, GWA and C-GWA. The crystal structure of C-WA, GWA, and C-GWA were characterized by an X-ray diffraction (XRD) analyzer (X'Pert Pro MPO) at a scan rate of 5° per minute in the angular range of 5°-90°. XPS spectra were obtained by an X-ray photoelectron spectroscopy (Thermofisher Scientific Escalab 250Xi, USA). Raman spectra with a laser excitation wavelength of 532 nm in the range of 1000–3000 cm^{-1} were obtained by LabRAM HR Evolution (Horiba Scientific LabRAM HR Evolution) at room temperature to characterize structural features of GWA and C-GWA.

2.6 Electromechanical performance test

For the testing of electromechanical performance of the pressure sensor, the pressure loading and high-precision control of displacement was carried out with a tensile testing machine (WNMC400, Beijing Wei Naguang Instrument Co., Ltd) to characterize electrical signal responses. The properties of electromechanical pressure sensors were determined using a digital source meter (Keithley 2450, U.S.A.) at a constant voltage of 1V.

3 Results And Discussion

3.1 Formation of C-GWA

The scheme of preparation process of C-GWA is shown in the Fig. 1. The shredded printing waste paper was changed into pulp after being oxidized by $NaClO_2$. Fiber bundles in the pulp are opened under vigorous stirring. Lignin and impurities in waste paper fibers are removed by chlorine dioxide produced by $NaClO_2$, which leads to a rough surface of the waste paper(Li et al. 2017b). Subsequently, waste paper fibers were dispersed in the ethanol dispersion of graphene to form a homogeneous suspension. The rough surface of the waste paper fiber provides adsorption sites which graphene in the ethanol is easily coated on. Afterward, the suspension was poured into a cylindraceous mould, filtered to yield the wet graphene coated waste paper aerogels, followed by drying directly at 60°C in an oven to obtain the graphene coated waste paper aerogel (GWA) under atmospheric pressure. The high aspect ratio and rough surface of waste paper fibers cause them to be easily entangled, forming a continuous 3D network. Graphene sheets are linked together to form a continuous conductive layer in the 3D network. Ethanol as a solvent in the suspension is essential for the drying process under the atmosphere because the surface tension of ethanol evaporation is too low to change the gap between the fibers. Therefore, the volume of the wet aerogel will not shrink and the aerogel structure will not collapse during drying(Li et al. 2017a). Compared with the vacuum freeze-drying and supercritical drying commonly used to prepare aerogels, drying under atmospheric condition only needs simple equipment and short time. For excellent compression space and mechanical behavior, cellulose in aerogels is generally annealed into carbon materials. Continuous porous structure of the aerogels is not only kept, but also the fiber diameter and the density of fiber entanglement points reduce which cause the decreased density and the increased compression space of the aerogel(Huang et al. 2021b; Sun et al. 2021a). Thus, GWA is annealed to the carbonized graphene coated waste paper aerogel (C-GWA) in a nitrogen atmosphere at 500°C to realize the characteristics of light weight and high compression. The carbon material converted from cellulose at 500°C has too low conductivity that cannot be measured (Shao et al. 2018), therefore, C-WA is not conductive. However, compared with C-WA, C-GWA has good conductivity provided by a continuous conductive layer formed by graphene.

3.2 SEM analysis

Surface morphology of C-WA, GWA and C-GWA is illustrated in Figs. 2a-2i. Figure 2a, 2d and 2g show that C-WA, GWA and C-GWA have porous and rough surface. Figure 2b, 2e and 2h show that C-WA, GWA and C-GWA have high aspect ratio of fibers and 3D structure of interpenetrated fibers. The rough surface is formed because the fibers inside the aerogel pass through the pores on the surface of the aerogel. It also can be seen from Fig. 2b, 2e and 2h that the diameter of fibers in C-WA and C-GWA is smaller than that of GWA because O, H and C elements escape from the fiber and fibers shrink during annealing. Figure 2c, 2f and 2i show the appearance of individual fiber in C-WA, GWA and C-GWA. The fiber in GWA exhibits rough surfaces due to the decomposition of lignin and other impurities by chlorine dioxide. The fiber in C-WA and C-GWA exhibits a regular wrinkle structure due to the escape of CO_2 and H_2O from the surface of the waste paper fiber during annealing. In addition, compared with the fiber in C-WA, graphene is evenly

coated on the surface of the fiber in GWA and C-GWA as shown in Fig. 2f and 2i. Figure 2j presents the photos of GWA and C-GWA. The specific shrinkage value of the volume is illustrated in Fig. 2k. The volume shrinkage rate is 24.2% when GWA is annealed to C-GWA. The volume of the aerogel shrinks after annealing due to the shrinkage of the fibers, which results in the shrinkage of the 3D skeleton formed by interpenetrated fibers. The density of GWA is 68.9mg/cm^3, however, the density of C-GWA is only 25mg/cm^3. Lower density of the C-GWA than GWA can be explained by the fact that the pyrolysis of cellulose leads to a large loss of mass of aerogel during annealing. Although the volume of carbon aerogel decreases, the mass per unit volume reduces.

3.3 XRD, XPS and Raman analyses

Figure 3a shows in the XRD spectra of GWA, C-WA and C-GWA. The characteristic peaks of GWA located at 14.9°, 22.57°, and 34.28° represent the crystal planes d_{101}, d_{002}, and d_{040} of cellulose I in the diffraction patterns of GWA(Wu et al. 2020). The characteristic peak of graphene is covered with the characteristic peak of cellulose at 22.57°. For C-GWA and C-WA, the characteristic peaks of cellulose at 14.9° and 34.28° disappear, and the diffraction peak at 22° becomes wide, representing the characteristic peak of amorphous carbon(Bi et al. 2014). Intensity of characteristic peak of C-GWA is higher than that of C-WA because the coating of graphene increases the content of ordered carbon. The result shows that the cellulose in waste paper fibers is successfully transformed to amorphous carbon during annealing. Figure 3b shows the Raman spectra of GWA and C-GWA. A G-band at ≈ 1580 cm^{-1} (related to crystalline sp^2 carbon) and a D-band at ≈ 1350 cm^{-1} (associated with defects or heteroatom doping) appear for GWA and C-GWA, indicating the successful coating of graphene on the fiber surface(Zhang et al. 2020b). The peak intensity of I_D/I_G of C-GWA is lower than that of GWA. This phenomenon can be explained by that the cellulose in waste paper fibers is transformed into amorphous carbon during annealing. Figures 3c shows XPS the spectra of GWA and C-GWA. The O/C atomic ratio of GWA is 0.315. However, the O/C atomic ratio of C-GWA is only 0.048, which suggests that most of the oxygen atoms in the GWA aerogel have been almost removed during annealing.

3.4 Mechanical performance of aerogels

Figure 4 shows the photos of C-GWA and GWA at different compression strains. GWA has obvious loss of height after recovery at different compression strains. However, C-GWA can return to the original height at low compressive strain, and height slightly reduces at high compressive strain. GWA returns to 95% of its original height at 10% compressive strain, however C-GWA completely returns to its original height. GWA and C-GWA return to 88% and 97% of its original height at a compressive strain of 30%, respectively. GWA and C-GWA returns to 88% and 91% of its original height at 50% compressive strain, respectively.

3.5 Electromechanical performance of the pressure Sensor

The schematic diagram of the wearable pressure sensor based on C-GWA is illustrated in Fig. 5a. The C-GWA are placed on an elastic tape with interdigitated electrodes. Figure 5b shows that the resistance of

the C-GWA-based pressure sensor varies with the increasing external pressure. The circuit is connected when the GCA-based pressure sensor is used as a touch sensitive switch. The brightness of LED strongly depends upon the compressive strain amplitudes. The higher the compressive strain is, the stronger the brightness of the LED lamp will be. Figure 5c to 5e show the relative current changes of the C-GWA-based pressure sensor in the pressure range from 16 Pa to 132 kPa where the relative current increases with the rise of pressure, certifying that the real-time current is highly sensitive to external pressure, which is attributed to the increasing contact area between the rough surface of the aerogel and the interdigital electrode. Additionally, the contact mode of graphene sheets is transformed from the edge-to-edge into the surface-to-surface under external pressure, which also leads to increased conductivity. Figure 5f shows the ultra-low detection capability of the C-GWA-based pressure sensor. A significant relative current change is observed when a green bean with a mass of 53.4 mg (≈ 2.5 Pa) is placed on the upper surface of the sensor due to the increase in pressure. The ability to detect ultra-low pressure is resulted from the rise of contact area between rough surface of the aerogel and the interdigital electrode under a smaller pressure. In addition, the wrinkle structure on the surface of the carbon fiber is easily connected under a small pressure, which will cause a change in resistance.

Sensitivity is an important index to evaluate the performance of wearable pressure sensors. The sensitivity (*S*) is defined and calculated based on the following formulas: $S = (\Delta I/I_0)/\Delta P$, where ΔI (A) is the relative change of current. I_0 (A) is the current without loading and ΔP (kPa) is the change of the applied pressure. As shown in Fig. 6, the C-GWA-based pressure sensor possesses a satisfyingly linear relationship between current response and applied pressure and has the sensitivity factors of S1 = 31.6 kPa^{-1} within 0.7 kPa stress, S2 = 7.3 kPa^{-1} for stress range of 0.7–3.5 kPa, and S3 = 3.12 kPa^{-1} over 3.5 kPa, respectively. It should be noted that the sensitivity of the low-pressure range is higher than that of the high-pressure range. In the low-pressure range, the increasing contact area between the aerogel and the electrode leads to a significantly reduced resistance. Simultaneously, the contact of wrinkle structures on the skeleton of the C-GWA also causes the resistance of the aerogel to decrease under small external pressure. As the pressure load rises, the sensitivity reduces because the rough surface of the aerogel fully contacts with the interdigital electrode and the aerogel is less and less susceptible to deformation due to the reduction in compressible space caused by increased pressure. Compared with other sensors based on 3D porous materials using graphene as a conductive filler reported in recent years, C-GWA-based pressure sensors have higher sensitivity and lower detection limit (Table S1), which is attributed to the changeable contact area between the C-GWA and the electrode and easily contacted wrinkle structures on the skeleton of the C-GWA. The reproducibility of the C-GWA-based sensor was evaluated through loading–unloading cyclic tests for 8000 cycles as shown in Fig. 6b, verifying the superior durability of the C-GWA-based pressure sensor. Figure 6c presents the relative current response of the C-GWA -based pressure sensor under 4538 Pa at various compression speeds of 0.5 mm/s, 1 mm/s and 2 mm/s, indicating the stability and repeatability of the pressure sensor under different compression speeds. Additionally, the sensor exhibits a fast response time of 176 ms and recovery time of 107 ms (Fig. 6d), ensuring its real-time feedback for external pressure. Figures 6e and 6f show the hydrophobic properties of C-GWA with a contact angle of up to 141° due to the removal of oxygen-containing functional groups

in the fiber during carbonization. Hydrophobicity contributes to application of the sensor based on C-GWA in humid environments.

3.6 The working mechanism of the pressure sensor.

Figure 7a shows the equivalent circuit diagram of the pressure sensor based on C-GWA. The total resistance of the pressure sensor is defined as $R_{total} = R_e + R_a + R_b$, where R_e is the electrode resistance and wire resistance, R_a is the contact resistance between the C-GWA and the electrode, and R_b is the bulk resistance of C-GWA. R_e remains unchanged with increasing external pressure, however, R_a, R_b and R_{total} is reduced. The variety of resistance and microstructural of the pressure sensor based on C-GWA under released and pressed states are further illustrated in Figs. 7b-d. For the sensor without pressure loading, there are many pores inside the aerogel and a gap between the aerogel and the electrode attributed to rough outer surface of the aerogel as shown in Fig. 7b. When the external pressure is applied, the deformed C-GWA achieved good contact to the electrode and pores within the aerogel are compressed, which causes fibers in C-GWA are compacted together. Additionally, the contact mode of the graphene sheets coated on the surface of the fibers is also transformed with the fibers in C-GWA aggregated (Fig. 7d). The edge-to-edge contact of the 2D graphene sheet is transformed into the surface-to-surface contact of the sheet. Figure 7c illustrates the process of contact between fibers in C-GWA. The wrinkle structure on the surface of the fiber comes into contact first in low-pressure stage. As the pressure enhances, the contact area between the fibers is enlarged. Resultly, the resistance of the C-GWA-based pressure sensor remarkably decreases. Pores inside C-GWA and the gap between C-GWA and the electrode are restored to their original size when the external pressure load is released, which cause the discontinuity of the conductive network and the resistance to return to its original value.

4 Application Of The Pressure Sensor In Human Motion Detection

The pressure sensor based on C-GWA are used for the detection of human motion under small and large deformation. The insulating tape was used to stick the sensor to different parts of the human body, and the inductive signal was measured and recorded by a multimeter. Figure 8a shows the C-GWA-based sensor can monitor real-time signal of the pulse of the human body. The radial arterial pulse waveform (P) peak and the systolic augmentation shoulder [T(D)] peak of the pulse is obvious in the small image. The C-GWA-based sensor shows great application prospects in human physiological monitoring. Figure 8b shows that different real-time signal is obtained when the bending angles of the finger are 0, 45 and 90°. The resistance value remains steady at each angle. The sensor also can be used to detect small deformation caused by cheek blowing (Figs. 8c) and large deformation caused by human body movement including neck bending, elbow bending, and knee joint bending (Figs. 8d to 8f). The sensor can show stability under various human motions, which proves the potential of the sensor in the field of smart wearable devices for human motion detection and linking to robots to imitate human behavior.

5 Conclusions

The aerogel based on graphene coated waste paper was successfully prepared by filtration and oven drying under atmospheric pressure, and further annealed to obtain the carbonized graphene coated waste paper aerogel (C-GWA). The C-GWA shows low density (25mg/cm^3), excellent compression resilience and outstanding performance. The wearable pressure sensor based on C-GWA displays a wide working range (0-132 KPa), high sensitivity (31.6 KPa^{-1}), fast response time (177ms) and good stability under 8000 cycles and different compression rates. In addition, the C-GWA-based pressure sensor can be applied to detect the pulse of the human body, cheek blowing and bending of human joints, which means potentially used in the field of wearable devices, and robots to imitate human behavior.

Declarations

Conflicts of interest

There are no conflicts of interest to declare

Acknowledgement

This work was financially supported by Sichuan Science and Technology Program (2021YFG0249), Cooperation Project between Sichuan University and Yibin City (2019CDYB-29), The National Natural Science Foundation of China and The Civil Aviation Administration of China (No. U1833118), and Engineering characteristic team of Sichuan University (2020SCUNG122).

References

1. Al-Azkawi A, Elliston A, Al-Bahry S, Sivakumar N (2019) Waste paper to bioethanol: Current and future prospective. Biofuel, Bioprod bior 13:1106-1118.
2. Bi H et al. (2014) Carbon microbelt aerogel prepared by waste paper: an efficient and recyclable sorbent for oils and organic solvents. Small 10:3544-3550.
3. Bi L, Yang Z, Chen L, Wu Z, Ye C (2020) Compressible AgNWs/Ti3C2Tx MXene aerogel-based highly sensitive piezoresistive pressure sensor as versatile electronic skins. J Mater Chem A 8:20030-20036.
4. Cao M, Su J, Fan S, Qiu H, Su D, Li L (2021) Wearable piezoresistive pressure sensors based on 3D graphene. Che Eng J 406:126777-12696.
5. Chen Y, Hu L, Li C, Dang B, Sun Q, Zhai T, Li H (2020a) A biomimetic-structured wood-derived carbon sponge with highly compressible and biocompatible properties for human-motion detection. InfoMat 2:1225-1235.
6. Chen Y et al. (2020b) Wood-Inspired Anisotropic Cellulose Nanofibril Composite Sponges for Multifunctional Applications. ACS Appl Mater Interfaces 12:35513-35522.

7. Chen Z, Zhuo H, Hu Y, Lai H, Liu L, Zhong L, Peng X (2020c) Wood-Derived Lightweight and Elastic Carbon Aerogel for Pressure Sensing and Energy Storage. Adv Funct Mater 30:1910292-1910303.
8. Das CM, Kang L, Ouyang Q, Yong KT (2020) Advanced low-dimensional carbon materials for flexible devices. InfoMat 2:698-714.
9. Ding Y, Xu T, Onyilagha O, Fong H, Zhu Z (2019) Recent Advances in Flexible and Wearable Pressure Sensors Based on Piezoresistive 3D Monolithic Conductive Sponges. ACS Appl Mater Interfaces 11:6685-6704.
10. Hodlur RM, Rabinal MK (2014) Self assembled graphene layers on polyurethane foam as a highly pressure sensitive conducting composite. Compos Sci Technol 90:160-165.
11. Huang J et al. (2019) Flexible electrically conductive biomass-based aerogels for piezoresistive pressure/strain sensors. Che Eng J 373:1357-1366.
12. Huang L, Chen J, Xu Y, Hu D, Cui X, Shi D, Zhu Y (2021a) Three-dimensional light-weight piezoresistive sensors based on conductive polyurethane sponges coated with hybrid CNT/CB nanoparticles. Appl Surf Sci 548:149268-149275.
13. Huang Y, Huang X, Ma M, Hu C, Seidi F, Yin S, Xiao H (2021b) Recent advances on the bacterial cellulose-derived carbon aerogels. J Mater Chem C 9:818-828.
14. Jin C, Han S, Li J, Sun Q (2015) Fabrication of cellulose-based aerogels from waste newspaper without any pretreatment and their use for absorbents. Carbohydr Polym 123:150-156.
15. Li L, Hu T, Sun H, Zhang J, Wang A (2017a) Pressure-Sensitive and Conductive Carbon Aerogels from Poplars Catkins for Selective Oil Absorption and Oil/Water Separation. ACS Appl Mater Interfaces 9:18001-18007.
16. Li L, Li B, Sun H, Zhang J (2017b) Compressible and conductive carbon aerogels from waste paper with exceptional performance for oil/water separation. J Mater Chem A 5:14858-14864.
17. Li Z, Shao L, Ruan Z, Hu W, Lu L, Chen Y (2018) Converting untreated waste office paper and chitosan into aerogel adsorbent for the removal of heavy metal ions. Carbohydr Polym 193:221-227.
18. Pang Y et al. (2018) Epidermis Microstructure Inspired Graphene Pressure Sensor with Random Distributed Spinosum for High Sensitivity and Large Linearity. ACS Nano 12:2346-2354.
19. Peng B, Zhao F, Ping J, Ying Y (2020) Recent Advances in Nanomaterial-Enabled Wearable Sensors: Material Synthesis, Sensor Design, and Personal Health Monitoring. Small 16:e2002681.
20. Salzano de Luna M, Wang Y, Zhai T, Verdolotti L, Buonocore GG, Lavorgna M, Xia H (2019) Nanocomposite polymeric materials with 3D graphene-based architectures: from design strategies to tailored properties and potential applications. Prog Polym Sci 89:213-249.
21. Shao Y, Guizani C, Grosseau P, Chaussy D, Beneventi D (2018) Biocarbons from microfibrillated cellulose/lignosulfonate precursors: A study of electrical conductivity development during slow pyrolysis. Carbon 129:357-366.
22. Si Y, Wang X, Yan C, Yang L, Yu J, Ding B (2016) Ultralight Biomass-Derived Carbonaceous Nanofibrous Aerogels with Superelasticity and High Pressure-Sensitivity. Adv Mater 28:9512-9518.

23. Sun Y, Chu Y, Wu W, Xiao H (2021a) Nanocellulose-based lightweight porous materials: A review. Carbohydr Polym 255:117489.
24. Sun Y et al. (2021b) Carbon aerogel reinforced PDMS nanocomposites with controllable and hierarchical microstructures for multifunctional wearable devices. Carbon 171:758-767.
25. Wang L, Zhang M, Yang B, Tan J, Ding X (2020) Highly Compressible, Thermally Stable, Light-Weight, and Robust Aramid Nanofibers/Ti3AlC2 MXene Composite Aerogel for Sensitive Pressure Sensor. ACS Nano 14:10633-10647.
26. Wei S, Qiu X, An J, Chen Z, Zhang X (2021) Highly sensitive, flexible, green synthesized graphene/biomass aerogels for pressure sensing application. Compos Sci Technol 207: 108730-108737.
27. Wei W, Qu X (2012) Extraordinary physical properties of functionalized graphene. Small 8:2138-2151
28. Wu R et al. (2020) Graphene decorated carbonized cellulose fabric for physiological signal monitoring and energy harvesting. J Mater Chem A 8:12665-12673
29. Wu ZY, Li C, Liang HW, Chen JF, Yu SH (2013) Ultralight, flexible, and fire-resistant carbon nanofiber aerogels from bacterial cellulose. Angew Chem Int Ed Engl 52:2925-2929.
30. Xiao Z et al. (2019) All-Carbon Pressure Sensors with High Performance and Excellent Chemical Resistance. Small 15:e1804779.
31. Yamaguchi A, Hiyoshi N, Sato O, Bando KK, Shirai M (2010) Gaseous fuel production from nonrecyclable paper wastes by using supported metal catalysts in high-temperature liquid water. ChemSusChem 3:737-741.
32. Ye T-N et al. (2015) Converting waste paper to multifunctional graphene-decorated carbon paper: from trash to treasure. J Mater Chem A 3:13926-13932.
33. Zhan Z et al. (2017) Paper/Carbon Nanotube-Based Wearable Pressure Sensor for Physiological Signal Acquisition and Soft Robotic Skin. ACS Appl Mater Interfaces 9:37921-37928.
34. Zhang P, Lv L, Liang Y, Li J, Cheng H, Zhao Y, Qu L (2016) A versatile, superelastic polystyrene/graphene capsule-like framework. J Mater Chem A 4:10118-10123.
35. Zhang Y et al. (2020a) Carbon nanotubes/acetylene black/Ecoflex with corrugated microcracks for enhanced sensitivity for stretchable strain sensors. J Mater Sci-Mater El 31:14145-14156.
36. Zhang Y et al. (2020b) Extremely stretchable strain sensors with ultra-high sensitivity based on carbon nanotubes and graphene for human motion detection. J Mater Sci-Mater El 31:12608-12619.

Figures

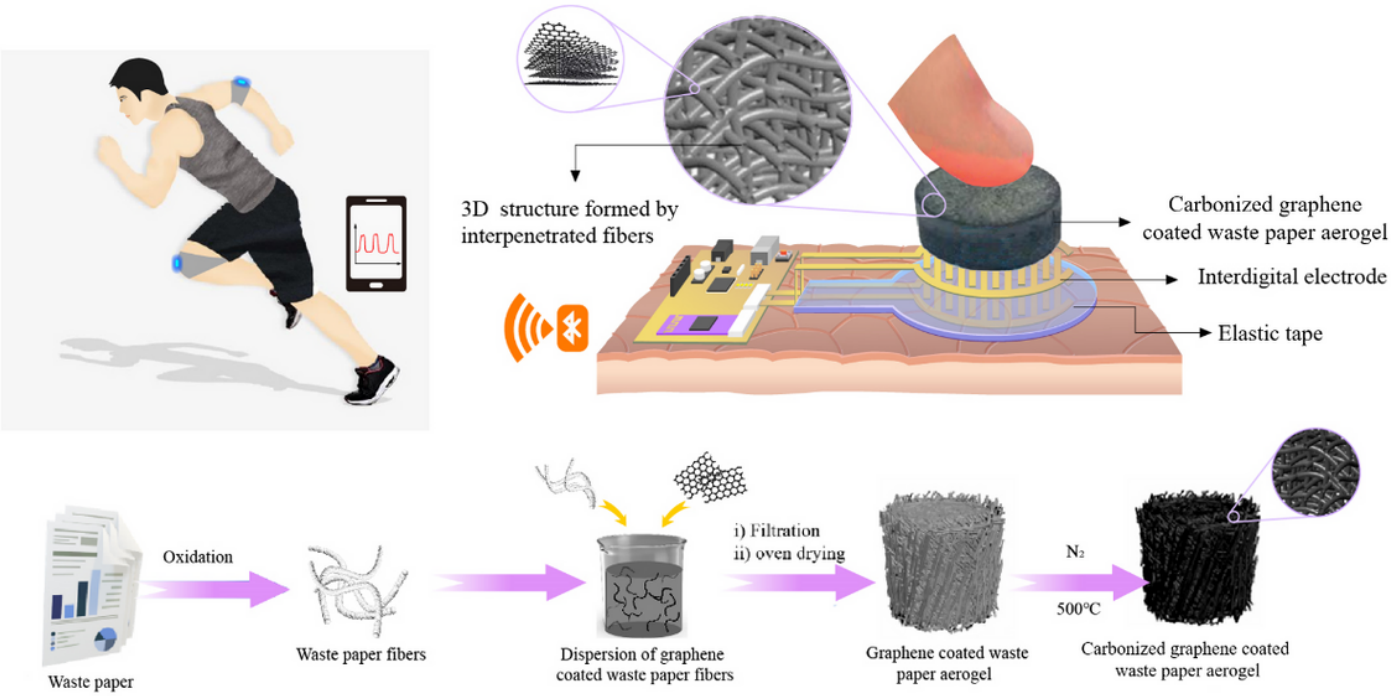

Figure 1

Schematic diagram of the formation of carbonized graphene coated waste paper aerogels (C-GWA).

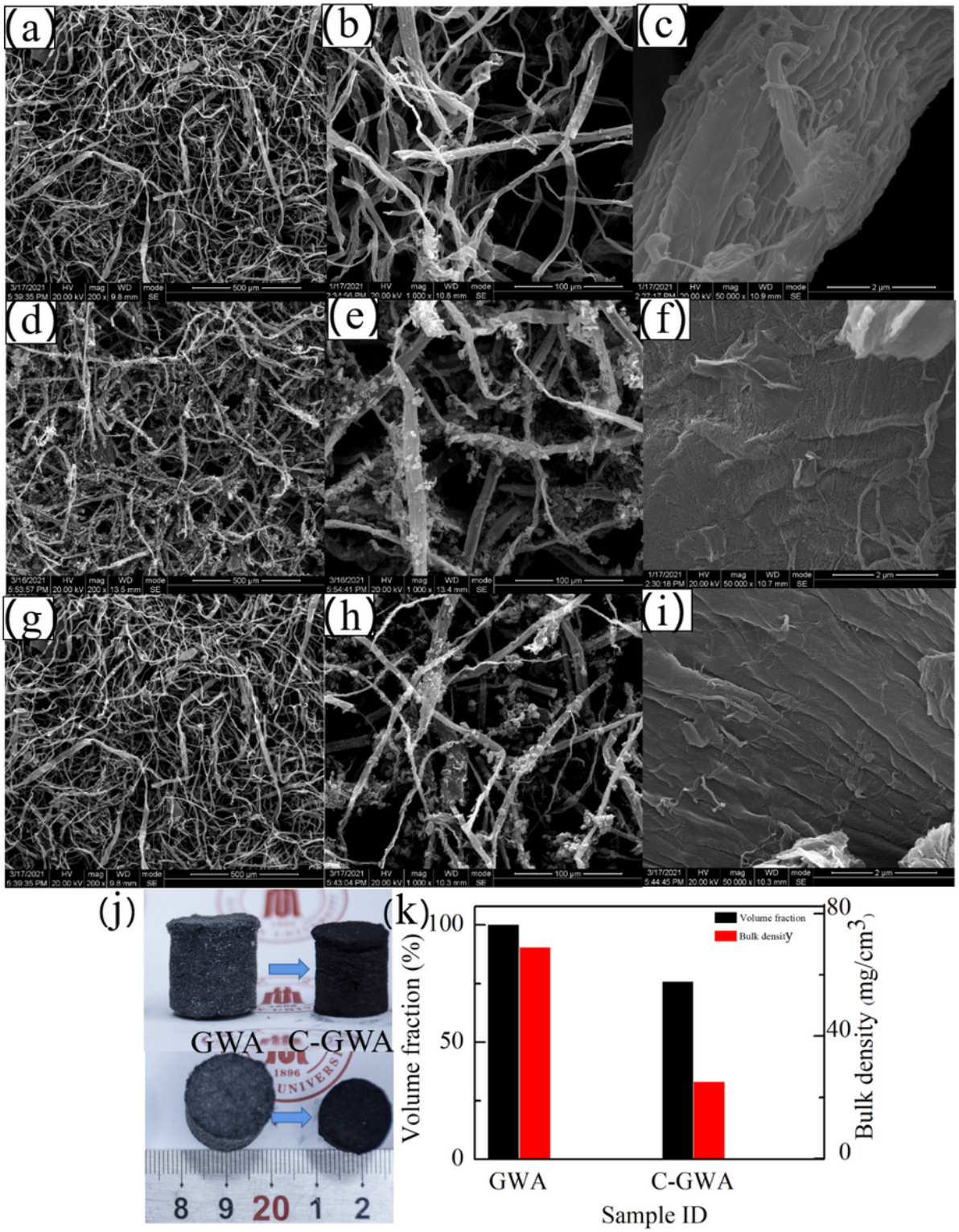

Figure 2

(a-c) SEM image of C-WA. (d-f) SEM image of GWA. (g-i) SEM images of C-GWA. (j) Photos of GWA and C-GWA. (k) Volume fraction and bulk density of GWA and C-GWA.

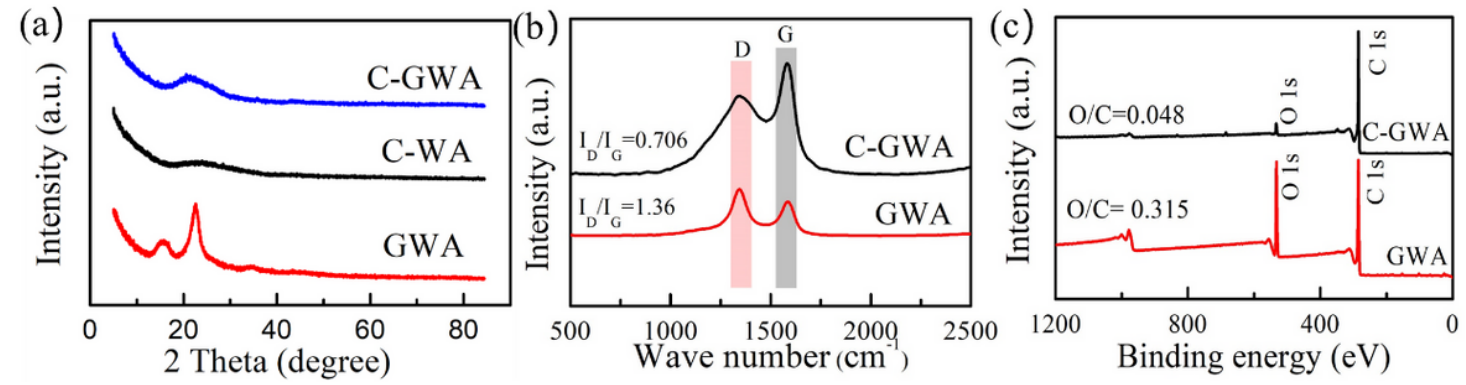

Figure 3

(a) XRD spectra of GWA, C-WA and C-GWA. (b) Raman spectra of WA, GWA and C-GWA. (c) XPS spectra of GWA and C-GWA.

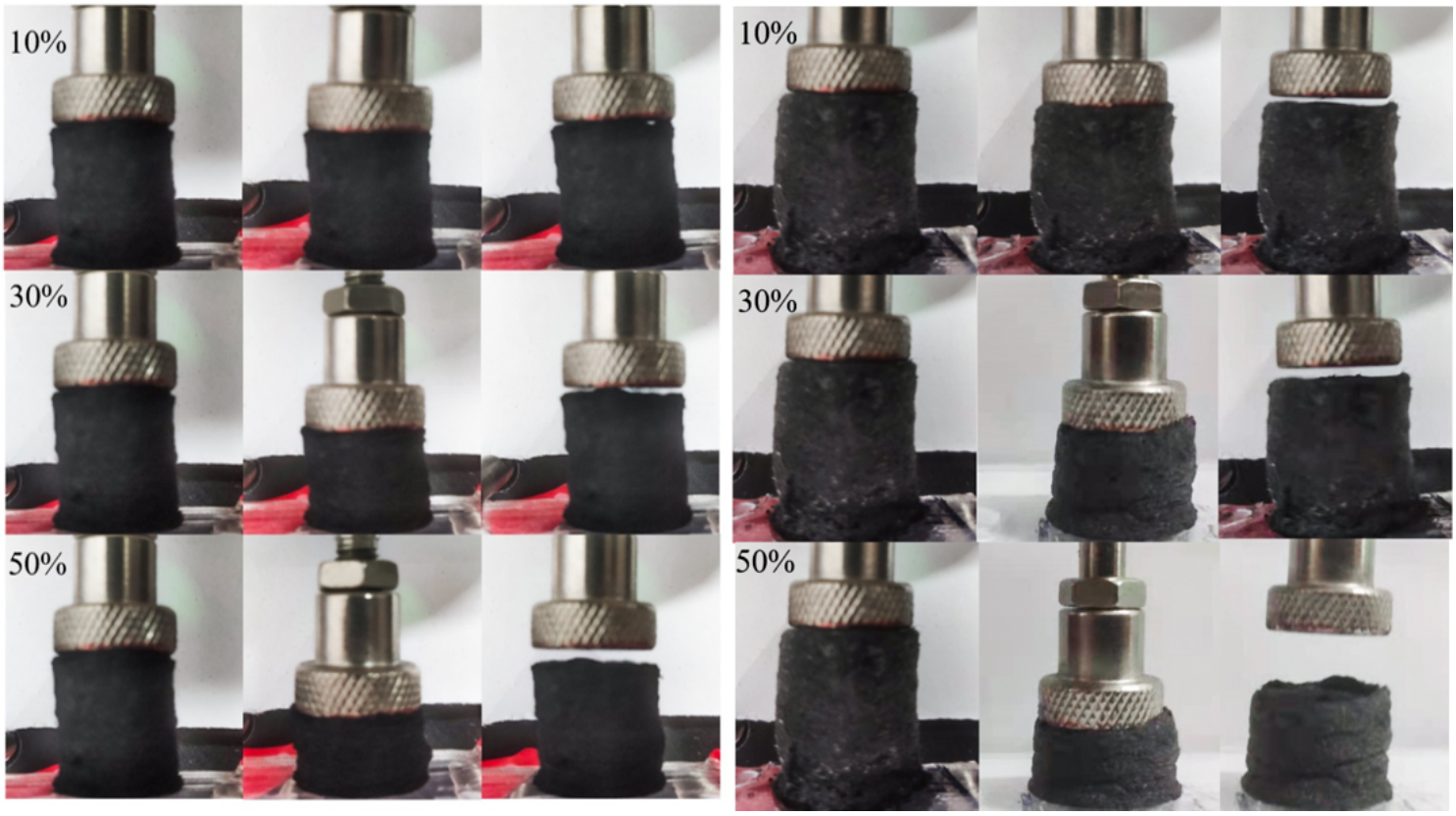

Figure 4

Photos of C-GWA (left) and GWA (right) at different compression strains.

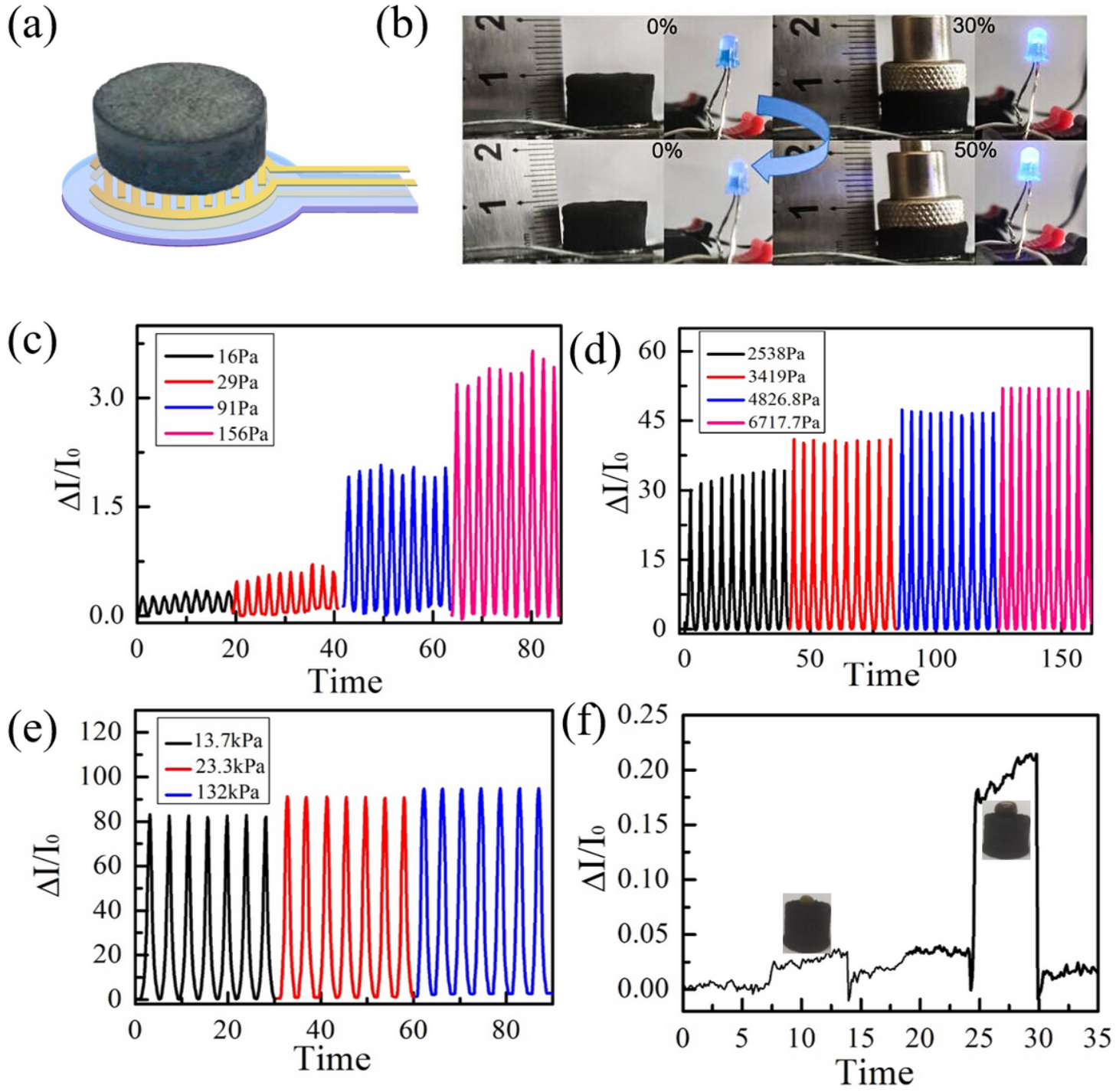

Figure 5

Electromechanical properties of the pressure sensor. (a) The schematic diagram of the C-GWA-based pressure sensor. (b) Brightness variation of the LED lamp under compression in the circuit based on the C-GWA-based pressure sensor. (c-e) Relative current change of C-GWA-based pressure sensor under cyclic pressing–releasing with various pressure loadings. (f) Relative current change of C-GWA-based pressure sensor under ultra-low pressure loadings.

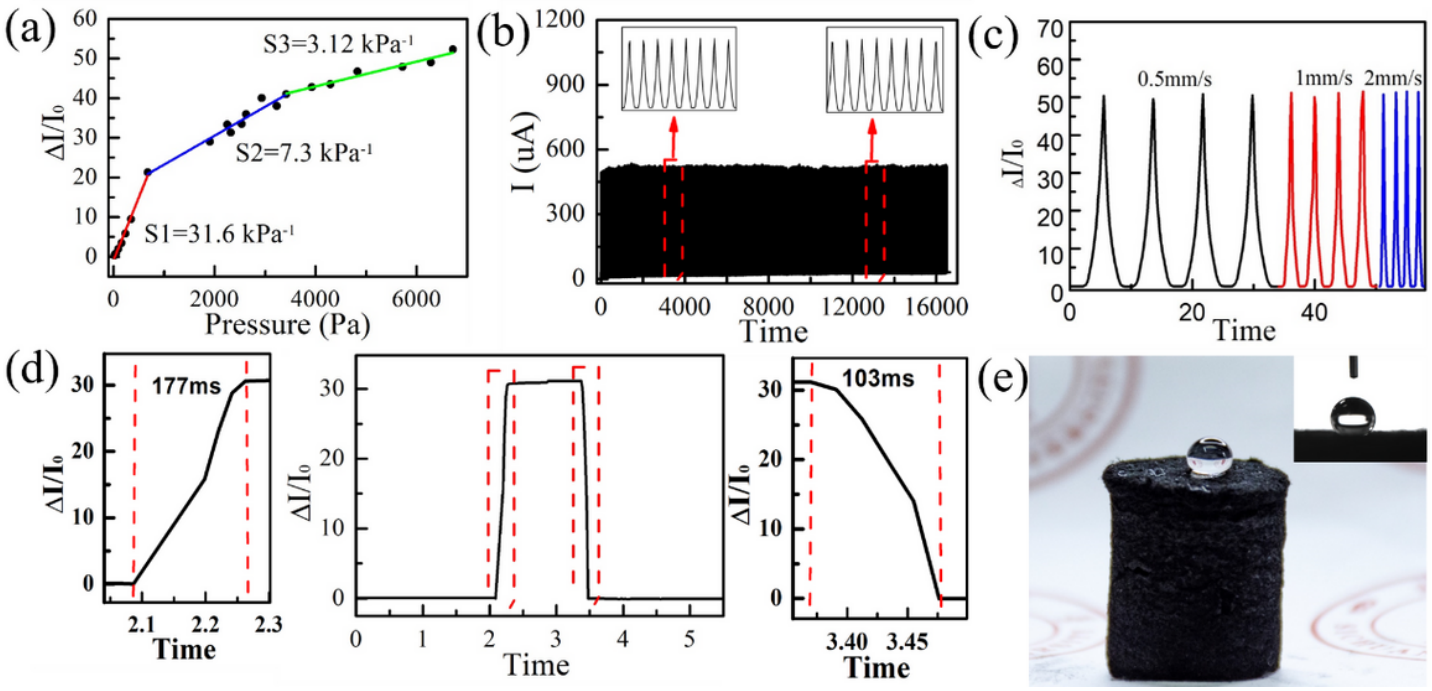

Figure 6

(a) Relative current change of C-GWA -based pressure sensor under pressure in the range from 0 kPa to 7kPa. (b) Relative current change of C-GWA-based pressure sensor under repeated loading-unloading with 8000 cycles. (c) Relative current change of C-GWA-based pressure sensor under different compression rates. (d) Response and recovery time of the C-GWA-based pressure sensor under compression and response. (e) Optical photograph of a water droplet on the surface of C-GWA.

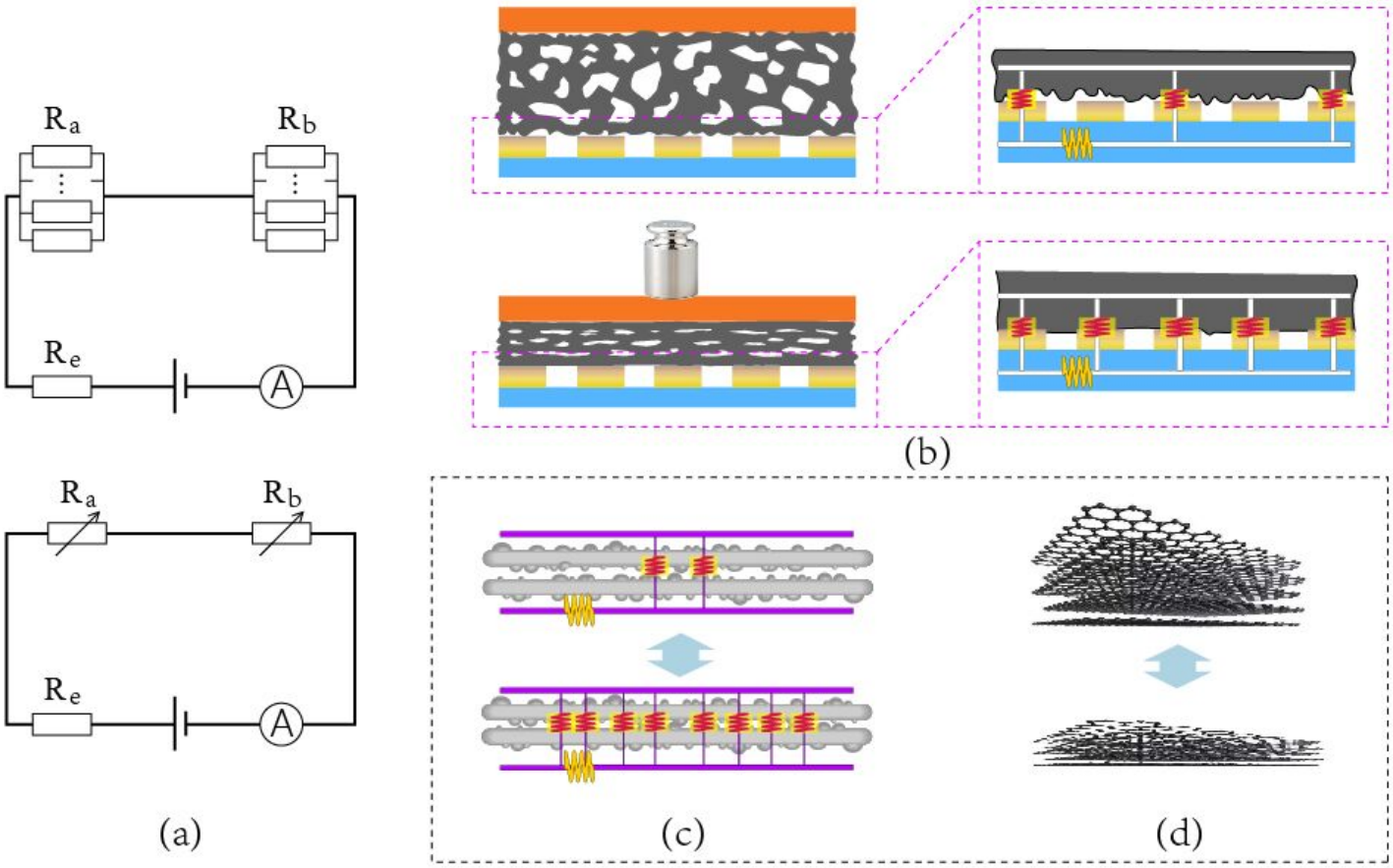

Figure 7

Schematic illustration of the working mechanism of the pressure sensor. (a) Equivalent circuit diagram of the pressure sensor. (b-d) Illustration of changes in the internal microstructure of the pressure sensor during pressing and releasing.

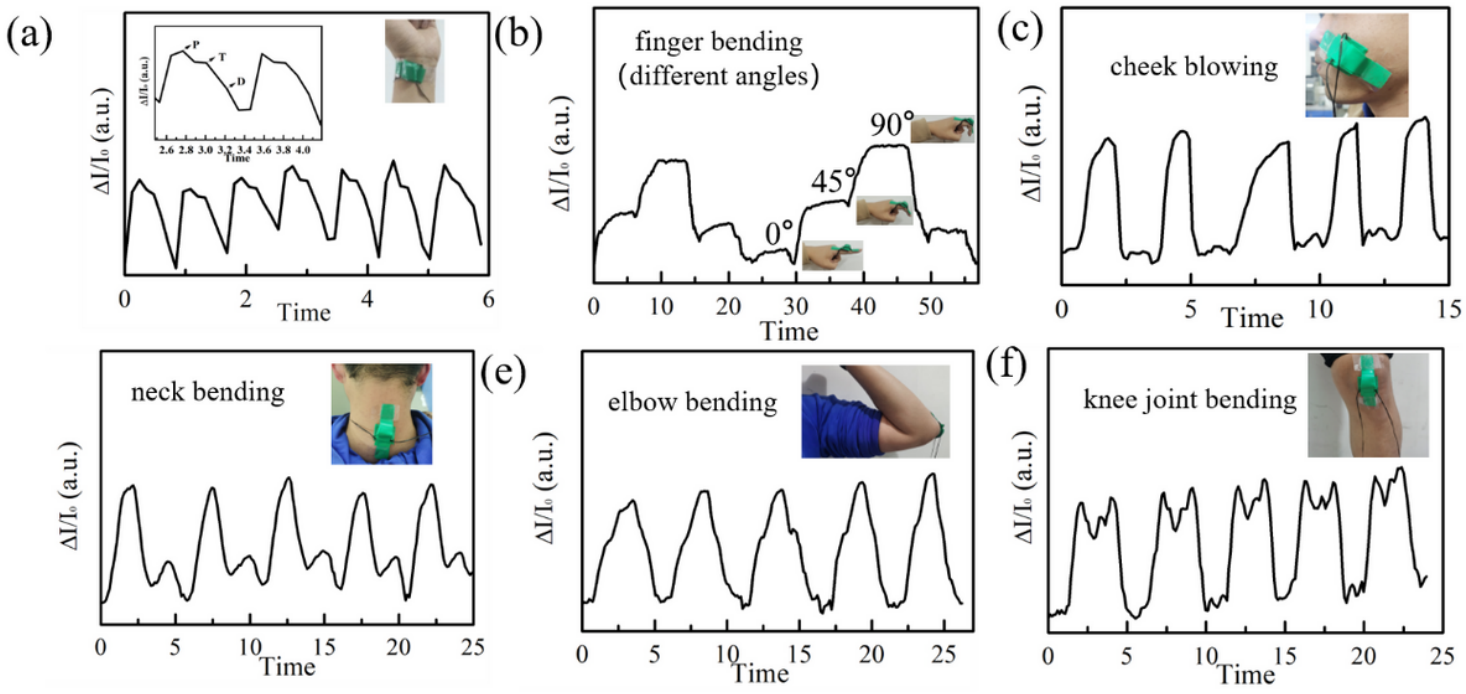

Figure 8

Applications of the C-GWA-based pressure sensor to detect: (a) human pulse (b) finger bending (different angles). (c) cheek blowing. (d) neck bending. (e) elbow bending. (f) knee joint bending.

Supplementary Files

This is a list of supplementary files associated with this preprint. Click to download.

- SupportingInformation.docx